JCTC Journal of Chemical Theory and Computation

An Efficient Real Space Multigrid QM/MM Electrostatic Coupling

Teodoro Laino,*[,†,‡] Fawzi Mohamed,[‡] Alessandro Laio,[‡] and Michele Parrinello[‡]

Scuola Normale Superiore di Pisa, Piazza dei Cavalieri 7, I-56125 Pisa, Italy, and Computational Science, DCHAB, ETH Zurich, USI Campus, Via Giuseppe Buffi 13, CH-6900 Lugano, Switzerland

Received May 3, 2005

Abstract: A popular strategy for simulating large systems where quantum chemical effects are important is the use of mixed quantum mechanical/molecular mechanics methods (QM/MM). While the cost of solving the Schrödinger equation in the QM part is the bottleneck of these calculations, evaluating the Coulomb interaction between the QM and the MM part is surprisingly expensive. In fact it can be just as time-consuming as solving the QM part. We present here a novel real space multigrid approach that handles Coulomb interactions very effectively and implement it in the CP2K code. This novel scheme cuts the cost of this part of the calculation by 2 orders of magnitude. The method does not need very fine-tuning or adjustable parameters, and it is quite accurate, leading to a dynamics with very good energy conservation. We exemplify the validity of our algorithms with simulations of water and of a zwitterionic dipeptide solvated in water.

Introduction

The rapid growth of computer technology has drastically changed the way in which molecular simulations and quantum chemical calculations are used to shed light on the driving forces of chemical reactivity in complex environments. However, the computational treatment of quantum systems made of several hundreds/thousands of atoms is still challenging,[1,2] especially if long simulation times are required. One of the currently followed strategies is the development of linear scaling quantum mechanical (QM) methods.[3−9] However, even with present-day hardware and the most efficient linear scaling method, it is not possible to study with fully ab initio methods many of the complex systems that are of current interest in biology and nanotechnology. An alternative approach is to employ multiscale quantum mechanics/molecular mechanics (QM/MM) schemes. They are particularly useful whenever a chemical reaction involves atoms in a small region, usually labeled QM. The QM part is treated with ab initio methods. The rest of the system, usually labeled MM, is instead treated with a less computationally expensive theory, generally molecular mechanics. Since the pioneering work of Warshel and Levitt,[10] the use and calibration of these techniques applied to the study of chemical reactivity has increased enormously.[11−18] Several quantum mechanics programs have been adapted to perform hybrid QM/MM simulations,[14,17,19−21] using either semiempirical,[20,22] ab initio Hartee-Fock,[19] post Hartree−Fock,[23] or DFT Hamiltonian.[14,17,19,24,25]

The study of chemical reactions in condensed phases is computationally demanding, owing not only to the size of the simulating system but also to the large degree of configurational sampling necessary to characterize a chemical reaction. This places severe demands on the efficiency of the implementation of any QM/MM scheme. Two main bottlenecks can be identified in such calculations: one concerns the evaluation of the QM energy and derivatives, while the other is associated with the evaluation of the electrostatic interaction between the QM and the MM part. In this respect we can identify two classes of codes, those based on Gaussian-type orbitals (GTOs) to represent both the wave function and the charge density[26,27] and those using

* Corresponding author fax: +41919138817; e-mail: teodoro.laino@sns.it. Corresponding author address: Computational Science, DCHAB, ETH Zurich, USI Campus, Via Giuseppe Buffi 13, CH-6900 Lugano, Switzerland.

† Scuola Normale Superiore di Pisa.

‡ Computational Science, DCHAB, ETH Zurich, USI Campus.

10.1021/ct050123f CCC: $30.25
Published on Web 10/07/2005

grids in real space to represent the charge density.[1,28,29] The latter encompasses both codes fully based on plane waves (PWs) and the more recent mixed approaches based on Gaussian plane waves (GPWs). It is on this second class of algorithms that our paper is focused.

For localized basis sets (GTOs), the use of an efficient prescreening technique is imperative in order to avoid the quadratic construction of the one-electron QM/MM Hamiltonian matrix. For nonlocal basis sets (PWs), if the interaction is evaluated analytically, the computational price is proportional to the number of grid points times the number of MM atoms. Surprisingly the evaluation of the QM/MM electrostatic interaction, for the latter scheme, requires between 20% and 100% of the time needed by the QM calculation, this despite the use of sophisticated hierarchical multipole (HMP) methods[24] or of clever implementations based on electrostatic cutoffs.[17] Furthermore these techniques require a fine-tuning of parameters to yield optimal performance and lead to a loss of accuracy that makes error control difficult.

The aim of this work is to describe a new implementation of the QM/MM coupling term that avoids the use of any hierarchical method or multipole technique. This novel scheme is based on the use of multigrid techniques in conjunction with the representation of the Coulomb potential through a sum of functions with different cutoffs, derived from the new Gaussian expansion of the electrostatic potential (GEEP for short). The QM/MM driver is based on the quantum mechanical program Quickstep and the molecular mechanics driver FIST (both part of the CP2K package).

The overall speedup is of 1−2 orders of magnitude with respect to other PW-based implementations of the QM/MM coupling Hamiltonian.[14,17] The lack of tuning parameters and electrostatic cutoffs makes this implementation a totally free parameter scheme, once the cutoff of the finest grid level has been specified. Consequently, very stable simulations can be obtained with optimal energy conservation properties.

We test the present implementation by computing the pair correlation function of quantum water in classical water and the pair correlation function of a zwitterionic dipeptide in classical water. Both tests address the correctness of the new coupling scheme.

Wave Function Optimization

We establish our implementation on the use of an additive[11,12,30] QM/MM scheme, where the total energy of the molecular system can be partitioned into three disjoint terms

$$E_{\mathrm{TOT}}(\mathbf{r}_\alpha,\mathbf{r}_a) = E^{\mathrm{QM}}(\mathbf{r}_\alpha) + E^{\mathrm{MM}}(\mathbf{r}_a) + E^{\mathrm{QM/MM}}(\mathbf{r}_\alpha,\mathbf{r}_a) \quad (1)$$

where E^{QM} is the pure quantum energy, E^{MM} is the classical energy, and $E^{\mathrm{QM/MM}}$ represents the mutual interaction energy of the two subsystems. These energy terms depend parametrically on the coordinates of the quantum nuclei ($\mathbf{r}_\alpha$) and classical atoms ($\mathbf{r}_a$).

The quantum subsystem is described at the density functional theory (DFT) level, exploiting the Quickstep[31] algorithm. This is based on the expansion of the Kohn−Sham orbitals in GTOs and on the use of an auxiliary PW basis set to evaluate the Coulomb interactions[31−33] and is included in the CP2K package.[1] Although the program has not been optimized to yield order N scaling for large systems, it is extremely fast and efficient in comparison with conventional DFT Gaussian or plane wave schemes for medium/large molecules. An extensive review of technical details and performance regarding Quickstep can be found in previous work.[31,34]

The classical subsystem is described through the use of the MM driver called FIST, also included in the CP2K package. This driver allows the use of the most common force fields employed in molecular mechanics simulations.[35,36]

The interaction energy term $E^{\mathrm{QM/MM}}$ contains all nonbonded contributions between the QM and the MM subsystem, and in a DFT framework we express it as

$$E^{\mathrm{QM/MM}}(\mathbf{r}_\alpha,\mathbf{r}_a) = \sum_{a\in \mathrm{MM}} q_a \int \frac{\rho(\mathbf{r},\mathbf{r}_\alpha)}{|\mathbf{r}-\mathbf{r}_a|} d\mathbf{r} + \sum_{\substack{a\in \mathrm{MM}\\ \alpha\in \mathrm{QM}}} \upsilon_{\mathrm{VdW}}(\mathbf{r}_\alpha,\mathbf{r}_a) \quad (2)$$

where $\mathbf{r}_a$ is the position of the MM atom a with charge q_a, $\rho(\mathbf{r},\mathbf{r}_\alpha)$ is the total (electronic plus nuclear) charge density of the quantum system, and $\upsilon_{\mathrm{VdW}}(\mathbf{r}_\alpha,\mathbf{r}_a)$ is the van der Waals interaction between classical atom a and quantum atom α. The implementation of the electrostatic $E^{\mathrm{QM/MM}}$ term poses serious theoretical and technical problems, related to both its short-range and its long-range behavior. An important issue, connected with the short-range behavior, is related to the so-called *electron spill-out* problem. In classical calculations the atoms are normally represented by a simple point charge. Whenever electrons of a QM atom come very close to the core of a classical atom, the electrons can be trapped into the pointlike classical potential energy source. The use of diffuse basis sets (or of plane waves) can enhance this behavior. A natural solution to this problem is to represent MM atoms with a finite width density of charge in the interaction with QM atoms. This width will be dependent on the atom type and can be expected to be similar to the covalent radius of the atom. The recently proposed implementation[17] describes the short-range interactions accurately, employing a pseudopotential-like approach to remedy the unphysical problem of overpolarization that arises when MM atoms are in close contact with the QM region.

To handle properly the short-range interaction we decided to use, rather than the functional form introduced by Laio et al.,[17] the following expression for the classical potential

$$\upsilon_a(\mathbf{r},\mathbf{r}_a) = \frac{\mathrm{Erf}\left(\frac{|\mathbf{r}-\mathbf{r}_a|}{r_{c,a}}\right)}{|\mathbf{r}-\mathbf{r}_a|} \quad (3)$$

where $r_{c,a}$ is an atomic parameter, close to the covalent radius of the atom a. This function is the exact potential energy function originated by a Gaussian charge distribution $\rho(\mathbf{r},\mathbf{r}_a) = (1/\sqrt{\pi}*r_{c,a})^3 \exp(-(|\mathbf{r}-\mathbf{r}_a|/r_{c,a})^2)$ and is commonly employed in the Ewald summation techniques. Moreover, the expression in eq 3 has the desired property of tending to $1/r$ at large distances and going smoothly to a constant for

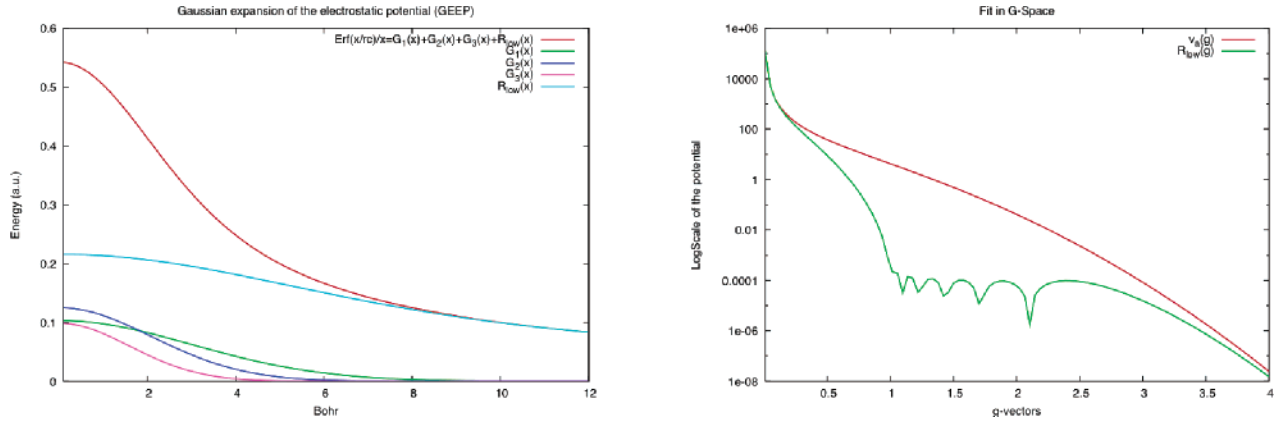

Figure 1. On the left: Gaussian expansion of the electrostatic potential (GEEP). The picture shows the components of the fit for the value $r_{c,a} = 1.1$ Å. On the right: Fourier transform of the potential in eq 3 (in red) and Fourier transform of the residual function R_{low} in eq 5 (in green). For this particular case ($r_{c,a} = 1.1$) we can define for the residual function a $G_{cut} \approx 1.0$.

small r. In the contest of QM/MM calculations,[37,38] the MM charges have been Gaussian smeared as a means to repair the broken covalent bonds at the QM/MM boundaries. In contrast here, we do not address the issue of treating QM/MM regions crossed by a covalent bond, and the smearing of all MM charges is exploited in order to prevent the spill-out problem and to accelerate the calculation of the electrostatic interactions.

Due to the Coulomb long-range behavior, the computational cost of the integral in eq 2 is surprisingly large. When using a localized basis set like GTOs, the most natural way to handle this term is to modify the one-electron Hamiltonian by adding to it the contribution of the MM classical field

$$H^{\mu\nu}_{\mathrm{QM/MM}} = -\int \phi_\mu(\mathbf{r},\mathbf{r}_\alpha) \sum_{a\in \mathrm{MM}} \frac{q_a}{|\mathbf{r}_a - \mathbf{r}|} \phi_\nu(\mathbf{r},\mathbf{r}_\alpha) d\mathbf{r} \qquad (4)$$

ϕ_μ and ϕ_ν being Gaussian basis functions and q_a the atomic charge of classical atom a with coordinates $\mathbf{r}_a$. In this case a suitable prescreening procedure has to be applied for the integral evaluation, to effectively compute only the nonzero terms and thus avoiding the quadratically scaling construction of the core Hamiltonian with respect to the number of elements of the basis set. When using a fully delocalized basis set like PWs, on the other hand, the QM/MM interaction term is evaluated by modifying the external potential and collocating on the grid nodes the contribution coming from the MM potential. Unfortunately the number of operations that a direct evaluation of eq 2 requires is of the order of $N_u N_{MM}$, where N_u is the number of grid points, usually of the order of 10^6 points, and N_{MM} is the number of classical atoms, usually of the order of 10^4 or more in systems of biochemical interest. It is evident that in a real system a brute force computation of the integral in eq 2 is impractical.

GEEP: Gaussian Expansion of the QM/MM Electrostatic Potential

The key to our method is the efficient decomposition of the electrostatic potential in terms of Gaussian functions with different cutoffs. The most general representation of the electrostatic potential eq 3 in terms of Gaussian functions with different cutoffs is

$$v_a(\mathbf{r},\mathbf{r}_a) = \frac{\mathrm{Erf}\left(\frac{|\mathbf{r}-\mathbf{r}_a|}{r_{c,a}}\right)}{|\mathbf{r}-\mathbf{r}_a|} = \sum_{N_g} A_g \exp\left(-\left(\frac{|\mathbf{r}-\mathbf{r}_a|}{G_g}\right)^2\right) + R_{low}(|\mathbf{r}-\mathbf{r}_a|) \qquad (5)$$

where the smoothed Coulomb potential is expressed as a sum of N_g Gaussian functions and of a residual function R_{low}. The A_g are the amplitudes of the Gaussian functions, and G_g are their width. If the parameters A_g and G_g are properly chosen, the residual function R_{low} will be smooth, i.e., its Fourier transform will have a compact domain for very small g vectors, and will be approximately zero for $g \gg G_{cut}$. The G_{cut} parameter is related to the spacing of the grid on which the R_{low} function will be mapped. We performed the fit of eq 5 by a least-squares approach in Fourier space, using the analytical expression of the **g**-representation of the modified electrostatic potential:[39]

$$\tilde{v}_a(\mathbf{g}) = \left[\frac{4\pi}{g^2}\right] \exp\left(-\frac{g^2 r_{c,a}^2}{4}\right) \qquad (6)$$

In Figure 1 we show the result of the fitting procedure in G-space with $r_{c,a} = 1.1$ Å, comparing the Fourier components of the modified Coulomb potential with the Fourier components of the residual function R_{low}. In this case the compact support of R_{low} is truncated at $G_{cut} \approx 1.0$ which should be compared with the value of $G_{cut} \approx 3.0$ needed to achieve the same accuracy when using $v_a(\mathbf{r},\mathbf{r}_a)$. This implies that the residual function can be mapped on a grid with a spacing 1 order of magnitude bigger than the one required to map the v_a function.

In Figure 1 we show the same result of the fit in real space, and in Table 1 we provide coefficients for selected values of $r_{c,a}$.

The advantage of this decomposition scheme is that grids of different spacing can be used to represent the different

Table 1. Amplitudes and Coefficients of the Optimal Gaussian Functions as Derived by the Fit

no. of Gaussians	radius $r_{c,a} = 1.1$ Å		radius $r_{c,a} = 0.44$ Å	
	A_g (au)	G_g (bohr)	A_g (au)	G_g (bohr)
1	0.103103	4.243060	0.230734	1.454390
2	0.125023	2.966300	0.270339	1.094850
3	0.098613	2.254250	0.075855	4.906710
4			0.190667	0.883485
5			0.173730	1.965640
6			0.127689	2.658160
7			0.095104	3.591640

contributions to $v_a(\mathbf{r},\mathbf{r}_a)$. In fact, the evaluation of a function on a grid relies on the assumption that the grid spacing is optimally chosen on the basis of its Fourier transform spectrum. Writing a function as a sum of terms with compact support and with different cutoffs, the mapping of the function is achieved using different grid levels, in principle as many levels as contribution terms, each optimal to describe the corresponding function. In our case, sharp Gaussians require fine grids, while coarser grids are necessary for the smoothest components. In addition the Gaussians can be truncated beyond a certain threshold value, which makes the collocation of the Gaussians on the grid a very efficient process.

The problem of mapping a noncompact function on a fine grid is then converted into the mapping of N_g compact functions on grids with cutoffs lower or at least equal to the fine grid, plus a noncompact very smooth function R_{low} mapped on the coarsest available grid. The sum of the contributions of the several grids, suitably interpolated, will be approximately equal to the function mapped analytically on the fine grid within errors due to the interpolation procedure.

Multigrid Framework

Multigrid methods are well-established tools in the solution of partial differential equations.[40,41] In the present implementation multigrid techniques are employed to combine functions with different cutoffs, i.e., represented on different grid levels.

Let us start by considering two grids, a coarse grid C with N_c points and a fine grid F with N_f points, whose grid-level is k-1 and k, respectively. The *interpolation* operator

$$I_{k-1}^{k}: C \rightarrow F \tag{7}$$

is by definition a transfer operator of a low cutoff function to a grid with a higher cutoff. The extension of the function to more points requires some regularity assumptions on its behavior. Two limiting cases can be identified: C^1 and C^∞, which can be handled with a simple linear interpolation scheme and with a *G-space* interpolation, respectively. If the function is C^∞, as in the case of a Gaussian, it is normally better to use an interpolator that assumes a high regularity. This ceases to be true once a collocation threshold is defined for the mapping of the Gaussians. In fact, the function on the grid becomes less regular, and an interpolation of a lower order might perform better. Another reason to avoid G-space interpolation comes from the fact that periodic boundary conditions with respect to the QM grid cannot be applied to the QM/MM potential. This makes the normal G-space interpolation unsuitable for our purpose. Thus we preferred to use an interpolation based on splines working entirely in real space unlike the scheme exploited by Yarne[16] et al. that relies on the use of splines in G-space. Moreover, the coding and the parallelization in real space is easier due to the use of commensurate grid levels and in our hands more efficient than working in G-space. For simplicity we use a set of commensurate grids, in which all the points of the coarse grid are points of the fine grid. Moreover, the number of points in each direction doubles going from the coarse to the fine grid level immediately above ($N_f = 8N_c$ in 3D). In the case of 1D space, the interpolation operator can be defined as

$$I_{k-1}^{k}(i,j) = \sum_n T(i,n)S^{-1}(n,j) \tag{8}$$

where for the points away from the border $T(i,n) = N_3(n-i/2)$ and $S(i,j) = N_3(j-i)$, with N_3 being the characteristic B-spline function of order 3.[42] The border was treated as a nonuniform B-spline. Higher dimensional spaces can be treated using the direct product of the transformation along the single dimensions. The opposite operation, the *restriction* J_k^{k-1}, is defined through the condition that the integral of the product of a function defined on the coarse grid with a function defined on a fine grid should give the same result both on the fine and on the coarse grid. Thus the restriction is simply the transpose of the interpolation

$$J_k^{k-1}(i,j) = [I_{k-1}^{k}(i,j)]^T = \sum_n S^{-1}(i,n)T(n,j) \tag{9}$$

Using N_{grid} grid levels and choosing the finer and coarser grid levels in order to treat correctly the sharpest and smoothest Gaussian components, respectively, we can achieve good accuracy and performance.

QM/MM Energy

The QM/MM electrostatic energy within DFT can be expressed with the following equation

$$E^{QM/MM}(\mathbf{r}_\alpha,\mathbf{r}_a) = \int d\mathbf{r}\rho(\mathbf{r},\mathbf{r}_\alpha)V^{QM/MM}(\mathbf{r},\mathbf{r}_a) \tag{10}$$

where $V^{QM/MM}$ is the electrostatic QM/MM potential evaluated on the finest grid, the same on which the final QM total density is evaluated. The overall description of the algorithm used to evaluate the QM/MM electrostatic potential on the finest grid can be outlined as follows:

(1) Each MM atom is represented as a continuous Gaussian charge distribution. The electrostatic potential generating from this charge is fitted through a Gaussian expansion using functions with different cutoffs, as shown in section 2.1.

(2) Every Gaussian function is mapped on one of the available grid levels, chosen to be the first grid whose cutoff is equal to or bigger than the cutoff of that particular Gaussian function. Using this collocation criterion, every

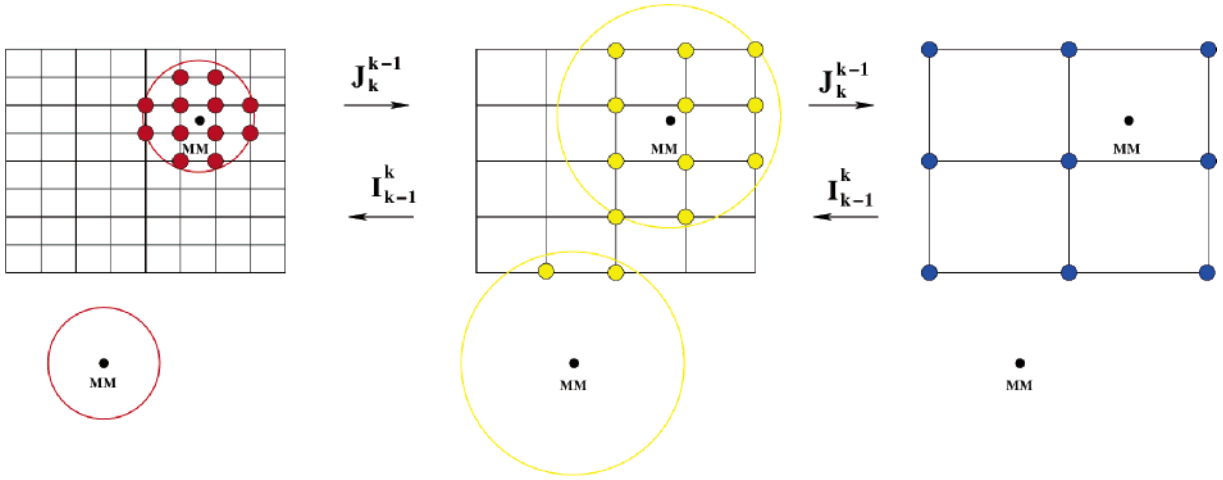

Figure 2. Schematic representation of the collocation procedure. Two MM atoms and three grid levels have been depicted. The circles (in the first and second grid levels) are the collocation regions of the Gaussian centered on the two MM atoms. Atoms whose distance from the QM box is greater than the Gaussian collocation radius do not contribute to the potential on that grid level. However, all atoms contribute to the coarsest grid level through the long-range R_{low} part.

Gaussian will be represented on the same number of grid points irrespective of its width. In practice a sub mesh of size $\approx 25 \times 25 \times 25$ suffices for an optimal Gaussian representation. Moreover, once a collocation threshold is defined, the Gaussian can be considered a compact domain function, i.e., it is zero beyond a certain distance, usually called a Gaussian radius. Thus only MM atoms embedded into the QM box, or close to it, will contribute to the finest grid levels, as shown in Figure 2.

The result of this collocation procedure is a multigrid representation of the QM/MM electrostatic potential $V_i^{QM/MM}(\mathbf{r},\mathbf{r}_a)$, where i labels the grid level, represented by a sum of single atomic contributions $V_i^{QM/MM}(\mathbf{r},\mathbf{r}_a) = \sum_{a\in MM} v_a^i(\mathbf{r},\mathbf{r}_a)$, on that particular grid level. In a realistic system the collocation represents most of the computational time spent in the evaluation of the QM/MM electrostatic potential, that is around 60−80%.

(i) Afterward, the multigrid expansion $V_i^{QM/MM}(\mathbf{r},\mathbf{r}_a)$ is sequentially interpolated starting from the coarsest grid level up to the finest level. The QM/MM electrostatic potential on the finest grid level can then be expressed as

$$V^{QM/MM}(\mathbf{r},\mathbf{r}_a) = \sum_{i=\text{coarse}}^{\text{fine}} \prod_{k=i}^{\text{fine}-1} I_{k-1}^{k}\, V_i^{QM/MM}(\mathbf{r},\mathbf{r}_a) \qquad (11)$$

where $V_i^{QM/MM}(\mathbf{r},\mathbf{r}_a)$ is the electrostatic potential mapped on grid level i, and I_{k-1}^{k} is the interpolation operator in real space. This operation does not depend on the number of MM atoms but only on the number of grid points, i.e., on the cutoff used in the calculation and on the dimensions of the QM box. For realistic systems the computational cost is around 20−40% of the overall cost of the evaluation of the QM/MM electrostatic potential.

Using the real space multigrid technique together with the GEEP expansion, the prefactor in the evaluation of the QM/MM electrostatic potential has been lowered from $N_f{*}N_f{*}N_f$ to $N_c{*}N_c{*}N_c$, where N_f is the number of grid points on the finest grid and N_c is the number of grid points on the coarsest grid. The computational cost of the other operations for evaluating the electrostatic potential, such as the mapping of the Gaussians and the interpolations, becomes negligible in the limit of a large MM system, usually more than 600−800 MM atoms.

Using the fact that grids are commensurate ($N_f/N_c = 2^{3(Ngrid-1)}$), and employing for every calculation 4 grid levels, the speed-up factor is around 512 (2^9); this means that the present implementation is 2 orders of magnitude faster than the direct analytical evaluation of the potential on the grid. The number of grid levels that can be used is limited by two technical factors. The first is that the coarsest grid needs to have at least as many points per dimension as the ones corresponding to the cutoff of the residual function R_{low} in order to perform the interpolation/restriction in an efficient manner. The second limitation is due to the constraint of using commensurate grid levels. The more grid levels are required in the calculation, the more the finest grid level cutoff will increase. This leads to an increment in memory requirements and to an unnecessary precision when handling the higher cutoff grids. Usually it is a combination of cutoff and grid levels that provides maximum efficiency. The two parameters can be chosen by checking that the coarsest grid level has no more than 5−10 grid points per dimension within the specified cutoff for the finest grid. Following the previous rule, the number of operations required for the direct evaluation of eq 2 is of the order of $N{*}100{*}N_{MM}$, where N is an integer between 1 and 10, and N_{MM} is the number of classical atoms.

QM/MM Energy Derivatives

The evaluation of the QM/MM derivatives on classical atoms are obtained by taking the derivative of eq 10 with respect to the classical atomic positions $\mathbf{r}_a$. These are given by

$$\frac{\partial E^{QM/MM}(\mathbf{r}_\alpha,\mathbf{r}_a)}{\partial_a} = \int d\mathbf{r}\rho(\mathbf{r},\mathbf{r}_\alpha)\frac{\partial V^{QM/MM}(\mathbf{r},\mathbf{r}_a)}{\partial \mathbf{r}_a} \qquad (12)$$

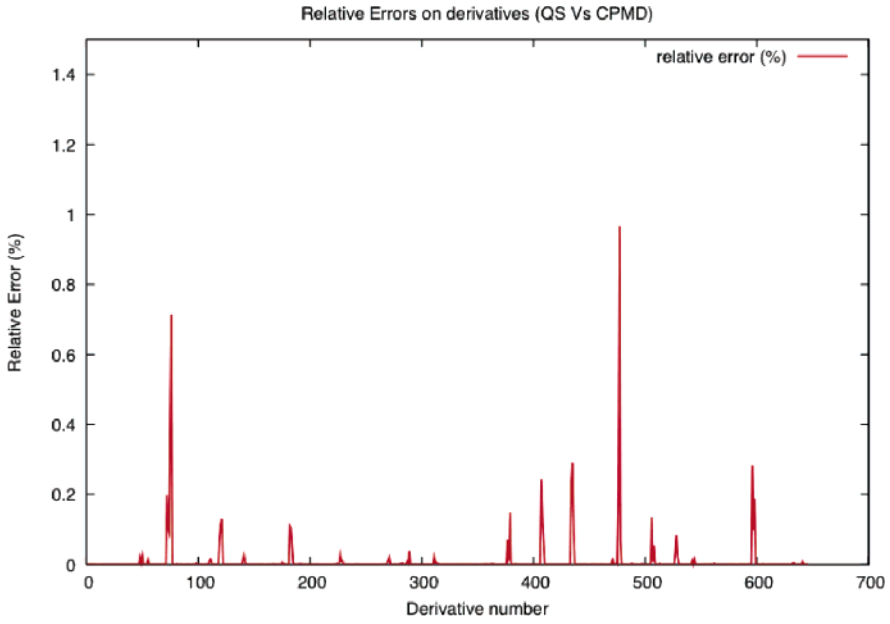

Figure 3. Relative errors on derivatives evaluated with the different functional form of eq 3 implemented in CPMD code and the new scheme implemented in CP2K. The average relative error is 0.01%.

The integral evaluation can be divided into terms deriving from the different grid levels

$$\frac{\partial E^{\mathrm{QM/MM}}(\mathbf{r}_\alpha,\mathbf{r}_a)}{\partial \mathbf{r}_a} = \sum_{i=\mathrm{coarse}}^{\mathrm{fine}} \int d\mathbf{r}\rho(\mathbf{r},\mathbf{r}_\alpha)\frac{\partial V_{\mathrm{fine}}^{i,\mathrm{QM/MM}}(\mathbf{r},\mathbf{r}_a)}{\partial \mathbf{r}_a} \tag{13}$$

where the $V_{\mathrm{fine}}^{i,\mathrm{QM/MM}}$ labels the potential term on the finest grid level coming from the corresponding grid level i. Using the multigrid expression for terms $V_{\mathrm{fine}}^{i,\mathrm{QM/MM}} = \prod_{k=i}^{\mathrm{fine}} I_{k-1}^{k}\, V_i^{\mathrm{QM/MM}}$, the derivatives on MM atoms can be written as

$$\frac{\partial E^{\mathrm{QM/MM}}(\mathbf{r}_\alpha,\mathbf{r}_a)}{\partial \mathbf{r}_a} = \sum_{i=\mathrm{coarse}}^{\mathrm{fine}} \int d\mathbf{r}\rho(\mathbf{r},\mathbf{r}_\alpha)\prod_{k=i}^{\mathrm{fine}-1} I_{k-1}^{k}\frac{\partial V_i^{\mathrm{QM/MM}}(\mathbf{r},\mathbf{r}_a)}{\partial \mathbf{r}_a} = \sum_{i=\mathrm{coarse}}^{\mathrm{fine}} \int d\mathbf{r}[\prod_{k=i+1}^{\mathrm{fine}} J_k^{k-1}]\rho(\mathbf{r},\mathbf{r}_\alpha)\frac{\partial V_i^{\mathrm{QM/MM}}(\mathbf{r},\mathbf{r}_a)}{\partial \mathbf{r}_a} \tag{14}$$

In the previous equation the property that the interpolation operator is equal to the transpose of the restriction operator (and vice versa) was used. The MM derivatives are then evaluated applying the restriction operator to the converged QM $\rho(\mathbf{r},\mathbf{r}_\alpha)$. This leads to a multigrid expansion of the density, and each integral is evaluated on the appropriate grid level. The overall derivative is the sum of the contributions of the different grid levels.

We now consider the forces on the QM atoms. If $n_c^\alpha(\mathbf{r})$ is the Gaussian density used to represent the core charge distribution of the αth quantum ions and labeling with $P^{\mu\nu}$ the $\mu\nu$ element of the density matrix in the Gaussian basis set $\{\phi_\mu\}$, the derivatives on quantum ions due to the QM/MM interaction potential are

$$\frac{\partial E^{\mathrm{QM/MM}}(\mathbf{r}_\alpha,\mathbf{r}_a)}{\partial \mathbf{r}_\alpha} = \sum_{\mu\nu}\left(\frac{\partial P^{\mu\nu}}{\partial \mathbf{r}_\alpha}\right)V_{\mu\nu}^{\mathrm{QM/MM}} + 2\sum_{\mu\nu} P^{\mu\nu}\int d\mathbf{r}\left(\frac{\partial \phi_\mu(\mathbf{r},\mathbf{r}_\alpha)}{\partial \mathbf{r}_\alpha}\right)V_{\mu\nu}^{\mathrm{QM/MM}}(\mathbf{r},\mathbf{r}_a)\phi_\nu(\mathbf{r},\mathbf{r}_\alpha) + \int d\mathbf{r}\left(\frac{\partial n_c^\alpha(\mathbf{r},\mathbf{r}_\alpha)}{\partial \mathbf{r}_\alpha}\right)V_{\mu\nu}^{\mathrm{QM/MM}}(\mathbf{r},\mathbf{r}_a) \tag{15}$$

where $V_{\mu\nu}^{\mathrm{QM/MM}} = \int d\mathbf{r}\phi_\mu(\mathbf{r},\mathbf{r}_\alpha)V^{\mathrm{QM/MM}}(\mathbf{r},\mathbf{r}_a)\phi_\nu(\mathbf{r},\mathbf{r}_\alpha)$ is the QM/MM Hamiltonian interaction term in the Gaussian basis set $\{\phi_\mu\}$. The first term is the so-called Pulay term[43] and is present because of the atom position dependent basis set.[31] The evaluation of the gradients on QM atoms is relatively inexpensive compared to a full quantum calculation. All considerations raised in section 3, regarding the scaling of the present scheme in the evaluation of the QM/MM potential, remain valid in the evaluation of the forces on classical atoms.

The calculation of the forces within the present implementation has been compared with the calculation of the forces using the method published elsewhere,[17] which is a QMMM of the CPMD code.[28] Comparison with the CPMD-QMMM code is complicated by the fact that in this last scheme[17] a multipolar expansion is used for the long-range part of the QM/MM electrostatic coupling, leading to inaccuracies. For this reason we compare only forces on atoms of the first MM solvation shell, which are treated exactly also in the CPMD-QMMM code. The realistic problem was made up of 215 classical SPC[44] water molecules and 1 QM water molecule. Although the system size is

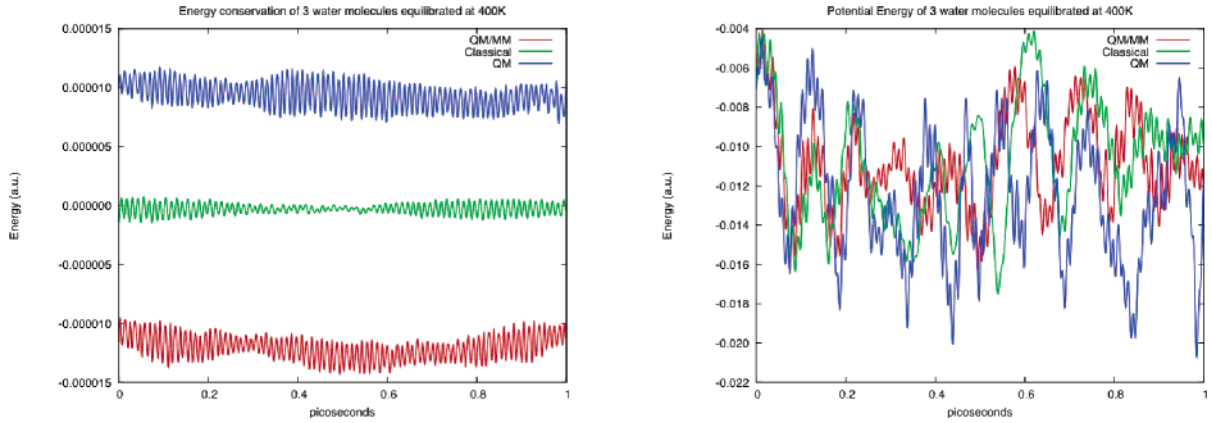

Figure 4. On the left: energy conservation of a system composed of 3 water molecules equilibrated at 400 K during 1 ps of simulation. The red line shows the total energy for the QM/MM run, the green line represents a pure classical run, and the blue line shows a pure quantum run. The total energies have been shifted for better visualization. No drift is observed, and all energy conservations are consistent. On the right: potential energy during the same run. Its variation is 3 orders of magnitude larger than the total energy variation.

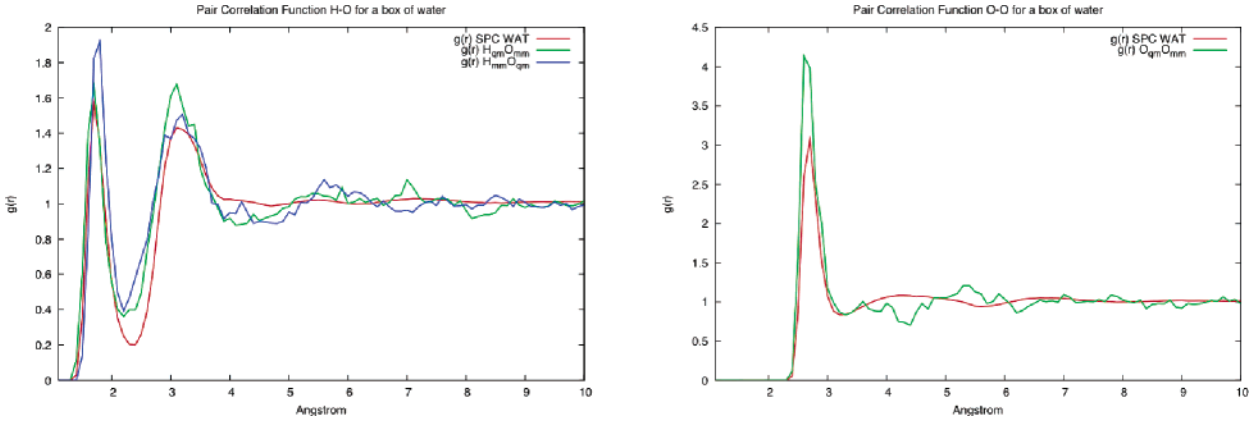

Figure 5. H−O and O−O pair correlation functions for QM water. QM/MM values are compared with the full classical SPC calculation. The QM/MM calculations are performed with $r_{c,a}$ equal to 1.2 Å for oxygen and 0.44 Å for hydrogen. The quantum box and the classical box employed in the simulation have a cube box size of 10.0 Å and 42.0 Å, respectively. The roughness of the QM/MM curve is due to the much shorter simulation time. The bin size for the evaluation of the pair correlation function is of 0.2 Å.

relatively small, the number of molecules present is comparable to the number of molecules normally treated exactly in CPMD-QMMM. In Figure 3 we show the relative error between the previous and the present implementations. The highest relative errors (less than 1.0%) correspond to forces that have small modules ($\leq 10^{-3}$ au). The average relative error is $\approx$0.01% with a speed-up in the energy and derivative evaluation of a factor of 40 wrt the CPMD.

An important benchmark for QM/MM codes that are aimed at molecular dynamics (MD) simulation is their ability to conserve energy. The system studied was composed of 3 water molecules (2 MM and 1 QM for the QM/MM run) previously equilibrated at 400 K. The simulation time was 1 ps, and results are shown in Figure 4. For comparison the energy of the pure classical and the quantum run are shown in the same picture. No drift is observed during 1 ps of simulation. We also show the potential energy during the simulation, whose oscillation is $\approx$3 orders of magnitude bigger than the total energy oscillation.

Results and Discussion

Consistently with checks done in previous work,[17,24] we test the accuracy of our implementation by computing the pair correlation function of a QM system embedded in a classical solvent. As found elsewhere,[17] the smoothing radius plays an important role in determining the bond properties of the system, and the choice of this parameter can have dramatic effects on pair correlation functions. The use of a different functional form (cf. eq 3 with eq 3 of Laio et al.[17]) forced us to reparametrize the $r_{c,a}$.

For the classical water molecules, the cutoff radii $r_{c,a}$ were chosen in order to reproduce the coordination number and the main peaks of the classical SPC water pair correlation function. A system of 2560 water molecules (2559 classical SPC water and 1 quantum water) in a cubic box, subject to periodic boundary conditions, was investigated. The system was previously equilibrated at $\rho = 1$ g/cm^3, $T = 298$ K. One SPC water molecule was then replaced by a QM water

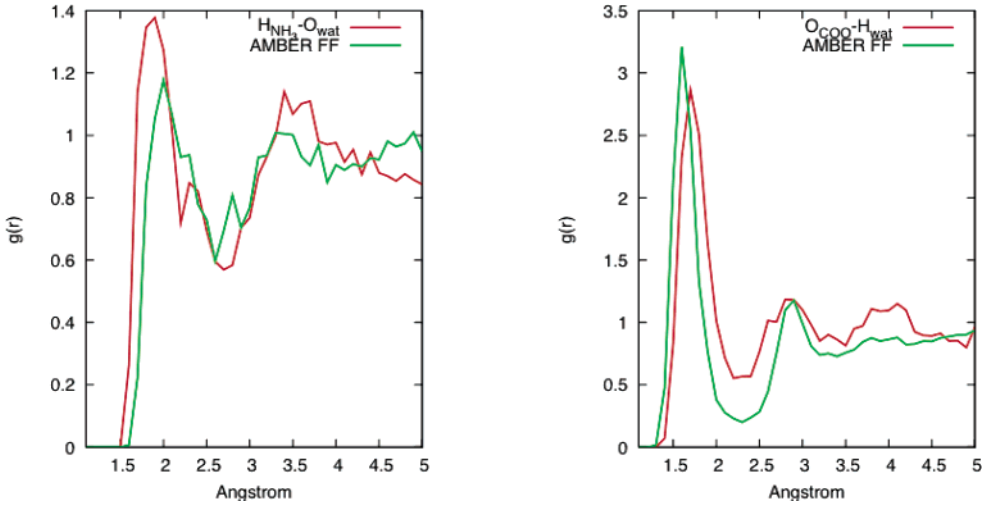

Figure 6. $H_{pept}-O_{wat}$ and $O_{pept}-H_{wat}$ pair correlation functions for the ALA-GLY dipeptide in SPC water. QM/MM values are compared with the full classical SPC calculation. The QM/MM calculations are performed with $r_{c,a}$ equal to 1.2 Å for oxygen and 0.44 Å for hydrogen. The quantum box and the classical box employed in the simulation have a cube box size of 15.0 Å and 50.0 Å, respectively. A plane-wave cutoff of 280 Hartree was used during all the simulations, in conjunction with the GTH pseudopotential and the BLYP exchange-correlation density functional. The roughness of the QM/MM curve is due to the much shorter simulation time. The bin size for the evaluation of the pair correlation function is of 0.2 Å.

molecule. GTH pseudopotentials[45] were used to describe the core charge distribution, and B-LYP exchange-correlation density functional[46,47] was employed in all the calculations, in conjunction with a cell plane-wave cutoff of $E_{cut} = 280$ Hartee. Several runs, with different values of the radius parameter $r_{c,a}$, were performed. The optimized radii are 0.44 Å for hydrogen and 1.20 Å for oxygen and allow the full classical SPC pair correlation function to be reproduced, as shown in Figure 5. Due to the different functional form of eq 3, the optimal values found with our implementation are different from the ones previously published.[17]

To test the transferability of the $r_{c,a}$ parameters determined for water, we also evaluated the pair correlation function of a QM dipeptide (GLY-ALA) zwitterion solvated in 3352 SPC water. We aimed at reproducing the pair correlation function obtained with the AMBER force field.[36] The pair correlation functions obtained with the present QM/MM implementation are indeed extremely close to the full classical results (see Figure 6).

Conclusions

We have presented an algorithm for evaluating the QM/MM coupling term with a fast linear scaling implementation. The main result is the dropping of the prefactor in the linear scaling, with a gain in the number of floating point operations proportional to $2^{3(N\text{grid}-1)}$, where N_{grid} is the number of grid levels used in the multigrid framework. The evaluation of the electrostatic potential on a grid is proportional to the number of MM atoms times the number of grid points. In real systems the linear scaling evaluation of the potential is therefore characterized by a prefactor $\approx 10^6$. In this scheme the prefactor is instead $\approx 10^3$. The number of floating point operations is reduced several orders of magnitude, and the computational time is 10−100 times smaller.

The algorithm is now implemented in the package CP2K, released under GPL license, and freely available on the Internet.[1] The scheme was validated by checking the energy conservation, and for a realistic system numerical accuracy was verified by comparing the forces with the analytical method, with a mean relative error of 0.01%. In addition, we computed the pair correlation function of a QM water molecule in classical water and of a QM zwitterionic dipeptide in classical water. The modified Coulomb interaction and the multigrid approach reproduce correctly the structural properties of a QM water molecule solvated in classical water and the parameters obtained therein can be used effectively to describe the properties of an organic molecule containing both negatively and positively charged moieties, as in the case of the zwitterion.

All tests address the correctness of results. The performance analysis confirms the present algorithm as the state of the art for the evaluation of QM/MM interaction coupling. Moreover, at variance with the majority of present-day QM/MM methods, our scheme does not rely on electrostatic cutoffs and so avoids all related problems. Consequently, the present method offers a fast, easy-to-use code for QM/MM calculations of large biological and inorganic systems.

Acknowledgment. The authors wish to thank Joost VandeVondele and Juerg Hutter for useful discussions and Christopher Mundy and William I-Feng Kuo for the very precious help they provided with the classical module FIST.

References

(1) Freely available at the URL: http://cp2k.berlios.de, released under GPL license.

(2) Head-Gordon, M. *J. Phys. Chem.* **1996**, *100*, 13213−13225.

(3) York, D.; Lee, T.; Yang, W. *Phys. Rev. Lett.* **1998**, *80*, 5011.

(4) Soler, J. M.; Artacho E.; Gale J. D.; Garcia A.; Junquera J.; Ordejon P.; Sanchez-Portal D. *J. Phys.: Condens. Matter* **2002**, *14*, 2745−2779.

(5) Gogonea, V.; Merz, K. M. *J. Phys. Chem. A* **1999**, *103*, 5171.

(6) Scuseria, G. E. *J. Phys. Chem. A* **1999**, *103*, 4782.

(7) Greatbanks, S. P.; Gready, J. E.; Limaye, A. C.; Rendell, A. P. *J. Comput. Chem.* **2000**, *21*, 788.

(8) Khandogin, J.; York, M. D. *J. Phys. Chem. B* **2002**, *106*, 7693.

(9) Krajewski, F.; Parrinello, M. *Phys. Rev. B* **2005**, *71* (23), Art. No. 233105.

(10) Warshel, A.; Levitt, M. *J. Mol. Biol.* **1976**, *103*, 227−249.

(11) Singh, U. C.; Kollman, P. A. *J. Comput. Chem.* **1986**, *7*, 718−730.

(12) Field, M. J.; Bash, P. A.; Karplus, M. *J. Comput. Chem.* **1990**, *11*, 700−733.

(13) Maseras, F.; Morokuma, K. *J. Comput. Chem.* **1995**, *16*, 1170−1179.

(14) Crespo, A.; Scherlis, D. A.; Martí, M. A.; Ordejon, P.; Roitberg, A. E.; Estrin, D. A. *J. Phys. Chem. B* **2003**, *107*, 13728−13736.

(15) Thompson, M. A. *J. Phys. Chem.* **1995**, *99*, 4794−4804.

(16) Yarne, D. A.; Tuckerman, M. E.; Martyna, G. J. *J. Chem. Phys.* **2001**, *115*, 3531−3539.

(17) Laio, A.; VandeVondele, J.; Rothlisberger, U. *J. Chem. Phys.* **2002**, *116*, 6941−6947.

(18) Nam, K.; Gao, J.; York, D. M. *J. Chem. Th. Comput.* **2005**, *1*, 2−13.

(19) Lyne, P. D.; Hodoscek, M.; Karplus, M. *J. Phys. Chem. A* **1999**, *103*, 3462−3471.

(20) Field, M. J.; Albe, M.; Bret, C.; Proust-De Martin, F.; Thomas, A. *J. Comput. Chem.* **2000**, *21*, 1088−1100.

(21) Sherwood, P.; de Vries, A. H.; Guest, M. F.; Schreckenbach, G.; Catlow, C. R. A.; French S. A.; Sokol, A. A.; Bromley, S.T.; Thiel, W.; Turner, A. J.; Billeter, S.; Terstegen, F.; Thiel, S.; Kendrick, J.; Rogers, S. C.; Casci, J.; Watson, M.; King, F.; Karlsen, E.; Sjøvoll, M.; Fahmi, A.; Schäfer, A.; Lennartz, C. *J. Mol. Struct. (THEOCHEM)* **2003**, *632*, 1−28

(22) Dewar, M. J. S.; Zoebisch, E. G.; Healy, E. A.; Stewart, J. J. P. *J. Am. Chem. Soc.* **1985**, *107*, 3902.

(23) Ferre, N.; Olivucci, M. *J. Am. Chem. Soc.* **2003**, *125*, 6868−6869.

(24) Eichinger, M.; Tavan, P.; Hutter, J.; Parrinello, M. *J. Chem. Phys.* **1999**, *110*, 10452−10467.

(25) Loferer, M. J.; Loeffler, H.H.; Liedl, K. R. *J. Comput. Chem.* **2003**, *24*, 1240−1249.

(26) Karlström, G.; Lindh, R.; Malmqvist, P.-A.; Roos, B. O.; Ryde, U.; Veryazov, V.; Widmark, P.-O.; Cossi, M.; Schimmelpfennig, B.; Neogrady, P.; Seijo, L. *Comput. Mater. Sci.* **2003**, *28*, 222.

(27) Schmidt, M. W.; Baldridge, K. K.; Boatz, J. A.; Elbert, S. T.; Gordon, M. S.; Jensen, J. H.; Koseki, S.; Matsunaga, N.; Nguyen, K. A.; Su, S.; Windus, T. L.; Dupuis, M.; Montgomery, J. A. *J. Comput. Chem.* **1993**, *14*, 1347−1363.

(28) Hutter, J.; Alavi, A.; Deutsch, T.; Ballone, P.; Bernasconi, M.; Focher, P.; Fois, E.; Goedecker, S.; Marx, D.; Parrinello, M.; Tuckerman, M. *CPMD v.9.1*; Technical Report; MPI für Festkörperforschung, Stuttgart and IBM: Zurich Research Laboratory, 2005.

(29) Fusti-Molnar, L.; Pulay, P. *J. Chem. Phys.* **2002**, *116*, 7795−7805.

(30) Sherwood, P. In *Modern Methods and Algorithms of Quantum Chemistry*; John von Neumann Institute for Computing: 2000; Chapter Hybrid quantum mechanics/molecular mechanics approaches, Vol. 1, pp 257−277.

(31) VandeVondele, J.; Krack, M.; Mohamed, F.; Parrinello, M.; Chassaing, T.; Hutter, J. *Comput. Phys. Comm.* **2005**, *167*, 103−128.

(32) Kohn, W.; Sham, L. *Phys. Rev.* **1965**, *140*, A1133−A1138.

(33) *Density Functional Theory of Atoms and Molecules*; Oxford University Press: New York, 1989.

(34) Lippert, G.; Hutter, J.; Parrinello, M. *Theor. Chem. Acc.* **1999**, *103*, 124−140.

(35) Lee, Y.; Hodoscek, M.; Brooks, B.; Kador, P. *Biophys. Chem.* **1998**, *70*, 203−216.

(36) Case, D.; et al. *AMBER v.7.0*; Technical Report; University of California: San Francisco, 2002.

(37) Amara, P.; Field M. J. *Theor. Chem. Acc.* **2003**, *109*, 43−52

(38) Das, D.; Eurenius, P. K.; Billings, E. M.; Sherwood, P.; Chatfield, C. D.; Hodoscek, M.; Brooks, B. R. *J. Chem. Phys.* **2002**, *117*, 10534−10547

(39) The Mathematica Notebook used to develop the GEEP technology is part of the CP2K distribution and can be freely downloaded. Released under GPL license.

(40) *Multi-Grid Methods and Applications;* Springer-Verlag: Berlin, 1985; Vol. 4 of *Series in Computational Mathematics.*

(41) *A Multigrid Tutorial*; SIAM Books: Philadelphia, PA, 1987.

(42) Feng, G. *IEEE Trans. Signal Process.* **1998**, *46*, 2790−2796.

(43) Pulay, P. *Mol. Phys.* **1969**, *17*, 197.

(44) *Intermolecular Forces*; Reidel: Dordrecht, The Netherlands, 1981; Chapter Interaction models for water in relation to protein hydration, pp 331−342.

(45) Goedecker, S.; Teter, M.; Hutter, J. *Phys. Rev. B* **1996**, *54*, 1703−1710.

(46) Becke, A. D. *Phys. Rev. A* **1988**, *38*, 3098.

(47) Lee, C.; Yang, W.; Parr, R. G. *Phys. Rev. B* **1988**, *37*, 785.

CT050123F